Journal of Molecular Liquids 259 (2018) 144–153

Contents lists available at ScienceDirect

Journal of Molecular Liquids

journal homepage: www.elsevier.com/locate/molliq

Novel ionic liquids incorporated pyridazinone-vanillyl motifs: Synthesis, characterization, pharmacological survey and molecular docking

Reda F.M. Elshaarawy [a,b,*], Mohamed H.A. Soliman [b], Mohamed A.-E. Zein [c], Zeinab H. Kheiralla [d], Douaa A. Abd El Bari [b]

[a] Institut für Bioanorganische Chemie, Heinrich-Heine Universität Düsseldorf, 40225 Düsseldorf, Germany
[b] Chemistry Department, Faculty of Science, Suez University, 43533 Suez, Egypt
[c] Chemistry Department, Faculty of Science, Damanhour University, Egypt
[d] Botany Department, University College for Women, Ain Shams University, Cairo, Egypt

ARTICLE INFO

Article history:
Received 31 January 2018
Accepted 6 March 2018
Available online 7 March 2018

Keywords:
Ionic liquids
Pyridazinone-vanillyl
Characterization
Antimicrobial
Docking study

ABSTRACT

Inspired by an urgent unmet medical need for development of potent and broad-spectrum antibiotics, we apply herein diverse strategies to obtain novel pyridazinone-vanillyl conjugates having a N(2)-arm of arylpropanamides (**8a**–**c**) or vanillyl ionic liquids (Val-ILs) (**9a**–**d**) motifs. These new pyridazinone-based antibiotic candidates display remarkable and broad-spectrum antimicrobial efficacy. Combined analysis of pharmacological results coupled with the *in Silico* derived parameters demonstrated the importance of the chemical nature of the arm in tuning the antimicrobial potency for the target compounds. For instance, **9b** (with Val-IL arm) (MIC/MBC = 1.98/2.18 μg/mL) is about 7-fold more potent than **8a** (with neutral arm) (MIC/MBC = 13.50/14.12 μg/mL) as Anti-*P. aeruginosa* agent. The molecular docking study revealed that compound **8a** was found to the most effective in binding to the active site of *E. coli* FabH (PDB code 1HNJ) with H-bonding, π-stacking and hydrophobic groove interactions having minimum binding energy $\Delta G_b = -14.00$ kcal/mol.

1. Introduction

Microbial infection is a serious problem worldwide and considered as one of the most important key health challenge which can be devastating due to its pathological impacts on clinical and community environment [1,2]. The antibiotics are pivotal to tackle the above challenge and indispensable for the sustainability of a healthy community free from microbial infections, however, overusing of these antibiotics for prolonged time leads to adaptation of bacteria against antibiotics and multidrug-resistant (MDR) [3,4]. Thus, it becomes imperative to explore novel antimicrobial drugs time-to-time to fight the bacterial infection and to negate this drug resistance. However, there are major challenges should be addressed for discovery and development of new antimicrobial drug such as steps of synthesis protocol, cost, and potential side effects.

Recently, the pyridazinone derivatives gain tremendous attention in the field of medicinal chemistry, because of their wide-range pharmacological activities including antibacterial [5], anticancer [6], antiHIV [7], antihypertensive [8,9], antidepressant [10], anticonvulsant [11], antithrombotic [12], cardiotonic [13] and diuretics [14]. Interestingly that some pyridazinone-based drugs such as minaprine [15], emorfazone [16], azanrinone [17], indolidan [18], bemoradan [19], primobendan [20] and levosimendan [21] are already sold in the clinical markets.

The amazing features of ionic liquids (ILs) such as low melting point, negligible vapor pressure, nonflammability, excellent mechanical and thermochemical stability, wide electrochemical avenue and supreme dual solubility in both organic and aqueous solvents [22] put them in the forefront of interest many researchers. Moreover, the amphiphilic nature of ILs may play a crucial role in controlling the pharmacokinetic properties, stability, delivery options, polymorphism of pharmacological agent, or even tuning pharmaceutical cocktails [23].

Inspired with the aforementioned remarks and in resumption of our ongoing programs directed toward the development of novel ILs-based potent and therapeutic agents [24,25] we report herein a synthesis protocol and *in vitro* antimicrobial evaluation of new vanillyl ILs-based pyridazinone derivatives with emphasize to develop a novel therapeutic strategy to combat antibiotic resistance for sustainable antimicrobial activity. Moreover, the docking simulations of the most potent compounds **8a** and **9b** with *E. coli* FabH (PDB code 1HNJ) were carried out to minimize the gap between the theoretical and actual view, also to understanding the interaction of the target compounds with *E. coli* FabH protein. The selection of FabH as antibacterial target was attributed to

* Corresponding author at: Institut für Bioanorganische Chemie, Heinrich-Heine Universität Düsseldorf, 40225 Düsseldorf, Germany.
E-mail addresses: reel-001@uni-duesseldorf.de, reda.elshaarawy@suezuniv.edu.eg (R.F.M. Elshaarawy).

https://doi.org/10.1016/j.molliq.2018.03.022
0167-7322/

that the fatty acid biosynthesis (FAB) act as the crucial metabolic process essential for the cell viability and the growth of bacterial strains [26]. Moreover, the initiation of this process is strongly correlated to the regulatory role for β-Ketoacyl-acyl carrier protein synthase III (FabH) [27] which is also important for initiating the FA elongation cycles and involved the feedback regulation of the biosynthesis pathway [28]. The structures of FabH proteins are highly conserved at the sequence in the gram-positive/-negative bacteria while no significantly homologous proteins are found in humans. Noteworthy, the active sites belong to various bacterial FabH molecules are basically invariant [29]. Consequently, FabH has confirmed to be a key target for the design of new antibiotics. Thus, a pharmacological agent which has the ability to inhibit the FabH enzymatic activity could be act as a promising candidate for selective, non-toxic, and broad-spectrum antibacterial agent.

2. Experimental section

2.1. Materials

See Supplementary data.

2.2. Instrumentation

See Supplementary data.

2.3. Synthesis

2.3.1. Synthesis of key starting materials (Val-ILs (**2a–d**) and pyridazinone 4)

See Supplementary data.

2.3.2. Synthesis of 4-(4-hydroxy-3-methoxybenzyl)-6-(4-methoxy-3-methylphenyl) pyridazin-3-one (**5**)

To a solution of KOH in absolute EtOH (25 mL, 5% w/v), compound **4** (0.9 g, 4.17 mmol) and vanillin (0.6 g, 4.17 mmol) were added. The mixture was refluxed under stirring for 2 h. After cooling, the mixture was concentrated *in vacuo*, diluted with cold water (25 mL), and acidified with 2 N HCl to pH = 2. After 1 h stirring in an ice-bath, compound **5** was completely precipitated, filtered off from the acidic solutions and recrystallized from ethanol. It was obtained as a dirty white solid (0.96 g, 65%); mp 198–199 °C; FT-IR (KBr) ν (cm^{-1}): 3408 (m, br), 3292 (m, br), 1661 (*vs*, sh). ^{1}H NMR (300 MHz, DMSO d_6): δ (ppm) 10.92 (s, 1H), 9.01 (s, 1H), 7.79–7.66 (m, 3H), 7.02–6.88 (m, 4H), 4.11 (s, 3H), 3.87 (s, 3H), 3.68 (s, 2H), 2.18 (s, 3H). ^{13}C NMR (75 MHz, DMSO d_6): δ (ppm) 165.50, 161.44, 155.42, 148.97, 145.80, 144.32, 133.68, 131.08, 128.32, 125.40, 122.59, 122.35, 119.84, 117.61, 116.28, 114.54, 58.02, 56.34, 43.03 and 20.57. EI-MS *m/z*: $[M]^+$ Calcd for $C_{20}H_{20}N_2O_4$ 352.38; Found 352.40. Anal. Calcd for $C_{20}H_{20}N_2O_4$ (M = 352.38 g/mol): C, 68.17; H, 5.72; N 7.95; Found: C, 67.98; H, 5.83; N 7.92.

2.3.3. Synthesis of methyl 3-(5-(4-hydroxy-3-methoxybenzyl)-3-(4-methoxy-3-methylphenyl)-6-oxopyridazin-1-yl)propanoate (**6**)

A mixture of the compound **5** (1.12 g, 2.68 mmol), K_2CO_3 (0.74 g, 5.36 mmol), and methyl bromopropionate (0.73 g, 4.02 mmol) in CH_3CN (20 mL) was refluxed under stirring for 3 h. The mixture was then concentrated *in vacuo*, diluted with cold water, and extracted with CH_2Cl_2 (3 × 25 mL). The solvent was evaporated *in vacuo*, and ester **6** was purified by column chromatography using cyclohexane/ethyl acetate 2:1 as an eluent. It was obtained as faint yellow crystals (0.68 g, 58%); mp 131–132 °C. FT-IR (KBr) ν (cm^{-1}): 3412 (m, br), 1740 (*vs*, sh) 1674 (s, sh); ^{1}H NMR (300 MHz, $CDCl_3$): δ (ppm) 11.40 (s, 1H), 7.68–7.54 (m, 3H), 7.05–6.85 (m, 4H), 4.05 (s, 3H), 3.89 (s, 3H), 3.71 (s, 3H), 3.57 (s, 2H), 3.38 (t, J = 8.4 Hz, 2H), 2.60 (t, J = 8.3 Hz, 2H), 2.30 (s, 3H). ^{13}C NMR (75 MHz, $CDCl_3$): δ (ppm) 175.38, 163.98, 158.76, 155.61, 148.51, 142.87, 141.36, 131.51, 130.08, 127.98, 125.85, 124.63, 122.88, 120.06, 116.69, 115.50, 114.39, 58.28, 56.41, 51.12, 46.98, 42.03, 32.91 and 20.55. EI-MS *m/z*: $[M]^+$ Calcd for $C_{24}H_{26}N_2O_6$ 438.47; Found 438.30. Anal. Calcd for (M = 438.47 g/mol): C, 65.74; H, 5.98; N, 6.39; Found: C, 65.59; H, 6.01; N, 6.33.

2.3.4. Synthesis of 3-(5-(4-hydroxy-3-methoxybenzyl)-3-(4-methoxy-3-methylphenyl)-6-oxopyrid-azin-1(6H)-yl)propanoic acid (**7a**)

A suspension of the ester **6** (1.16 g, 2.66 mmol) in 6 N NaOH (20 mL) was stirred at 60 °C for 1 h. The mixture was diluted with cold water and acidified with 6 N HCl with stirring in an ice-bath, the acid **7a** was isolated, filtered off and then recrystallized from ethanol. It was obtained as white crystals (0.78 g, 69%); mp 185–186 °C. FT-IR (KBr) ν (cm^{-1}): 3396 (m, br), 1698 (*vs*, sh), 1676 (s, sh). ^{1}H NMR (300 MHz, $CDCl_3$): δ (ppm) 11.79 (s, 1H), 10.88 (s, 1H), 7.72–7.59 (m, 2H), 7.11–6.98 (m, 3H), 6.84–6.72 (m, 2H), 3.99 (s, 3H), 3.87 (s, 3H), 3.63 (s, 2H), 3.21 (t, J = 8.1 Hz, 2H), 2.75 (t, J = 8.1 Hz, 2H), 2.28 (s, 3H). ^{13}C NMR (75 MHz, $CDCl_3$): δ (ppm) 175.68, 162.63, 158.81, 156.13, 148.11, 142.98, 141.46, 131.12, 130.03, 128.06, 125.82, 124.56, 122.71, 120.05, 116.69, 115.63, 114.42, 57.39, 56.70, 48.12, 43.22, 33.44 and 20.01. EI-MS *m/z*: $[M]^+$ Calcd for $C_{23}H_{24}N_2O_6$ 424.16; Found 424.10. Anal. Calcd for $C_{23}H_{24}N_2O_6$ (M = 424.16 g/mol): C, 65.08; H, 5.70; N, 6.60; Found: C, 65.01; H, 5.78; N, 6.49.

2.3.5. General procedure for aminolysis of pyridazinone propanoic acid (**7a**) with aromatic amines: synthesis of amides (**8a–c**)

To a cooled (−5 °C) and stirred solution of pyridazinone propanoic acid (**7a**) (0.254 g, 0.60 mmol) in anhydrous tetrahydrofuran (6 mL), Et_3N (2.10 mmol) was added. After 30 min, the mixture was allowed to warm up to 0 °C and ethyl chloroformate (0.66 mmol) was added. After 1 h, the commercially available substituted arylamine (1.20 mmol) was added. The reaction was stirred at room temperature for 12 h, then the mixture was concentrated *in vacuo*, diluted with cold water (20–30 mL) and then extracted with CH_2Cl_2 (3 × 15 mL). The solvent was evaporated to obtain final compounds (**8a–c**) which were purified by column chromatography using cyclohexane/ethyl acetate 2:1 and *n*-hexane/ethyl acetate 3:2 as eluents. Samples of the isolated products were characterized as follow;

2.3.5.1. 3-(5-(4-Hydroxy-3-methoxybenzyl)-3-(4-methoxy-3-methylphenyl)-6-oxopyridazin-1(6H)-yl)-N-(4-(trifluoromethyl)phenyl)propanamide (**8a**)

Obtained as a yellow powder (0.20 g, 58%); mp 239–241 °C. FT-IR (KBr) ν (cm^{-1}): 3298 (m, br), 1689 (*vs*, sh), 1676 (s, sh). ^{1}H NMR (300 MHz, DMSO d_6): δ (ppm) 11.06 (s, 1H), 8.99 (s, 1H), 7.79–7.71 (m, 3H), 7.67 (dt, J = 4.1, 2.4 Hz, 2H), 7.47–7.33 (m, 4H), 6.97 (dd, J = 8.4, 1.6 Hz, 2H), 4.02 (s, 3H), 3.92 (s, 3H), 3.69 (s, 2H), 3.49 (t, J = 8.3 Hz, 2H), 2.59 (t, J = 8.3 Hz, 2H), 2.18 (s, 3H). ^{13}C NMR (75 MHz, DMSO d_6): δ (ppm) 176.34, 161.70, 160.30, 156.03, 151.15, 148.69, 146.11, 142.64, 138.47, 136.61, 132.55, 132.12, 130.72, 128.83, 127.77, 127.47, 126.35, 124.31, 121.97, 118.90, 116.71, 115.46, 113.17, 111.45, 59.88, 57.28, 48.02, 43.14, 31.45 and 20.51. EI-MS *m/z*: $[M]^+$ Calcd for $C_{30}H_{28}F_3N_3O_5$ 567.56; Found 567.50. Anal. Calcd for $C_{30}H_{28}F_3N_3O_5$ (M = 567.56 g/mol): C, 63.49; H, 4.97; N, 7.40; Found: C, 63.38; H, 4.98; N, 7.36.

2.3.5.2. 3-(5-(4-Hydroxy-3-methoxybenzyl)-3-(4-methoxy-3-methylphenyl)-6-oxopyridazin-1(6H)-yl)-N-(4-methoxyphenyl)propanamide (**8b**)

Obtained as a faint yellow solid (0.24 g, 62%); mp: 218–219 °C. FT-IR (KBr) ν (cm^{-1}): 3210 (m, br), 1686 (*vs*, sh), 1666 (s, sh). ^{1}H NMR (300 MHz, DMSO d_6): δ (ppm) 11.08 (s, 1H), 8.99 (s, 1H), 7.79–7.66 (m, 4H), 7.47–7.33 (m, 5H), 6.97–6.85 (m, 2H), 4.23 (s, 3H), 4.02 (s, 3H), 3.92 (s, 3H), 3.76 (s, 2H), 3.49 (t, J = 8.1 Hz, 2H), 2.59 (t, J = 8.1 Hz, 2H), 2.18 (s, 3H). ^{13}C NMR (75 MHz, DMSO d_6): δ (ppm) 176.98, 161.64, 161.05, 158.24, 151.83, 148.09, 145.51, 141.42, 139.03, 136.96, 136.44, 134.53, 131.28, 129.15, 127.82, 127.50, 126.09, 123.25, 121.92, 120.13, 118.11, 117.21, 112.78, 111.77, 64.08, 60.12, 58.34, 49.15, 42.47, 31.71 and 19.27. EI-MS *m/z*:

$[M]^+$ Calcd for $C_{30}H_{31}N_3O_6$ 529.58; Found 529.50. Anal. Calcd for $C_{30}H_{31}N_3O_6$ (M = 529.58 g/mol): C, 68.04; H, 5.90; N, 7.93; Found: C, 67.91; H, 5.96; N, 7.91.

*2.3.5.3. N-(2,4-dimethoxyphenyl)-3-(5-(4-hydroxy-3-methoxybenzyl)-3-(4-methoxy-3-methyl phenyl)-6-oxopyridazin-1(6H)-yl)propanamide (**8c**).* Obtained as a yellowish-white solid (0.29, 63%); mp 238–240 °C. FT-IR (KBr) ν (cm^{-1}): 3225 (m, br), 1684 (s, sh), 1665 (s, sh). ^1H NMR (300 MHz, DMSO d_6): δ (ppm) 11.07 (s, 1H), 9.00 (s, 1H), 7.80–7.74 (m, 2H), 7.69–7.66 (m, 1H), 7.48–7.34 (m, 5H), 6.99–6.85 (m, 2H), 4.21 (s, 3H), 4.11 (s, 3H), 3.93 (s, 3H), 3.77 (s, 3H), 3.59 (s, 2H), 3.46 (t, J = 7.9 Hz, 2H), 2.76 (t, J = 7.9 Hz, 2H), 2.20 (s, 3H). ^{13}C NMR (75 MHz, DMSO d_6): δ (ppm) 176.39, 169.47, 161.82, 158.66, 157.76, 154.86, 148.84, 146.20, 143.47, 141.50, 132.57, 130.68, 129.54, 128.45, 125.81, 123.62, 122.82, 119.74, 118.32, 115.96, 114.85, 107.38, 101.23, 58.34, 57.78, 55.97, 55.57, 51.15, 49.69, 42.80, 42.80, 40.03, 39.76, 39.48, 39.20, 38.92, 31.49 and 19.16. EI-MS m/z: $[M]^+$ Calcd for $C_{31}H_{33}N_3O_7$ 559.61; Found 559.60. Anal. Calcd for $C_{31}H_{33}N_3O_7$ (M = 559.61 g/mol): C, 66.53; H, 5.94; N, 7.51; Found: C, 66.52; H, 5.96; N, 7.38.

*2.3.6. Synthesis of 3-(5-(4-hydroxy-3-methoxybenzyl)-3-(4-methoxy-3-methylphenyl)-6-oxo-pyridazin-1-yl)propanehydrazide (**7b**)*

To an ethanolic solution of methyl pyridazinone-2-ylpropanoate derivative (**6**) (4.39 g, 0.01 mol), hydrazine hydrate (99%) (3 mL) was added and the mixture was stirred under reflux for 3 h. The obtained precipitate was filtered off, washed with water, dried and recrystallized from ethanol to give a yellowish-white solid (3.11 g, 71%); mp: 201–202 °C. FT-IR (KBr) ν (cm^{-1}): 3421 (m, br), 3307, 3293 (m, sh), 3188 (m, sh), 1681 (*vs*, sh), 1668 (s, sh). ^1H NMR (300 MHz, DMSO d_6): δ (ppm) 10.92 (s, 1H), 10.18 (s, 1H), 7.71–7.67 (m, 3H), 7.09–6.88 (m, 4H), 3.87 (s, 3H), 3.78 (s, 3H), 3.58 (s, 2H), 3.26 (t, J = 8.2 Hz, 2H), 2.68 (t, J = 8.2 Hz, 2H), 2.27 (s, br, 2H), 2.05 (s, 3H). ^{13}C NMR (75 MHz, DMSO d_6): δ (ppm) 183.68, 161.89, 158.65, 156.17, 148.24, 143.02, 141.67, 131.52, 130.33, 127.78, 125.94, 124.77, 122.83, 118.95, 116.67, 114.91, 114.36, 57.25, 56.52, 47.99, 42.87, 32.47 and 19.86. EI-MS m/z: $[M]^+$ Calcd for $C_{23}H_{26}N_4O_5$ 438.48; Found 438.20. Anal. Calcd for $C_{23}H_{26}N_4O_5$ (M = 438.48 g/mol): C, 63.00; H, 5.98; N, 12.78; Found: C, 62.79; H, 6.01; N, 12.65.

*2.3.7. General procedure for synthesis of ionic liquids-based pyridazinohydrazones (**9a–d**)*

Into a 100 mL Schlenk flask, an ethanolic solution (10 mL) of vanillyl ionic liquids (**2a–d**) (2.0 mmol) was added dropwise to a solution (20 mL) of propanehydrazide (**7b**) (0.88 g, 2.0 mmol) in ethanol under N_2 atmosphere. The reaction mixture was refluxed with stirring under N_2 for 3 h. Then the solvent was partially removed in rotatory evaporator, and yellow products (**9a–d**) were departure from the solution by the addition of ethyl acetate along with keeping in the refrigerator overnight. Then the solvent was decanted off and the isolated crude product was sonicated for 15 min in Et_2O (3 × 25 mL). Et_2O was also decanted off and the residual solid was washed intensively with EtOH/Et_2O mixture (1:2) to remove unreacted materials and then re-dissolved in EtOH. EtOAc was added slowly (during ~15 min) to precipitate the products as yellow solids which were collected by filtration and dried under vacuum. Samples of the isolated products were characterized as follow;

*2.3.7.1. 1-(4-Hydroxy-3-((2-(3-(5-(4-hydroxy-3-methoxybenzyl)-3-(4-methoxy-3-methyl phenyl)-6-oxopyridazin-1(6H)-yl)propanoyl) hydrazono)methyl)benzyl)-4-methoxy pyridinium chloride (**9a**).* Obtained as a yellow powder, yield (1.06 g, 76%); mp = 230–231 °C. FT-IR (KBr) ν (cm^{-1}): 3425 (m, br), 3194 (m, sh), 1677 (*vs*, sh), 1665 (s, sh), 1599 (s, sh), 1556 (m, sh), 1273 (s, sh), 1145 (s, sh), 748 (m, sh), 565 (m, sh). ^1H NMR (300 MHz, DMSO d_6): δ (ppm) 11.28 (s, 1H), 10.65 (s, 1H), 8.99 (d, J = 3.2 Hz, 2H), 8.79 (s, 1H), 8.32 (s, 1H), 7.78 (dd, J = 7.2, 2.6 Hz, 3H), 7.67 (q, J = 4.1, 3.3 Hz, 2H), 7.51–7.29 (m, 6H), 6.96 (dd, J = 8.5, 1.7 Hz, 2H), 4.90 (s, 2H), 4.39 (s, 2H), 4.22 (s, 3H), 3.99 (s, 3H), 3.83 (s, 3H), 3.77 (s, 3H), 3.61 (s, 2H), 3.03 (t, J = 7.0 Hz, 2H), 2.65 (t, J = 7.0 Hz, 2H), 2.09 (s, 3H). ^{13}C NMR (75 MHz, DMSO d_6): δ (ppm) 128.22, 165.13, 162.30, 157.75, 150.87, 149.72, 148.13, 144.44, 139.25, 137.03, 135.41, 132.86, 129.71, 129.58, 128.99, 128.48, 125.87, 124.49, 123.67, 121.09, 117.97, 117.43, 117.11, 116.53, 116.17, 115.44, 113.70, 64.18, 58.51, 57.15, 55.64, 54.79, 50.49, 42.19, 33.62 and 22.26. ESI-MS m/z: $[M - Cl^-]^+$ Calcd for $C_{38}H_{40}N_5O_8$ 694.75; Found 694.70. Anal. Calcd for $C_{38}H_{40}ClN_5O_8$ (M = 730.21 g/mol): C, 62.50; H, 5.52; N, 9.59; Found: C, 62.39; H, 5.55; N, 9.49.

*2.3.7.2. 1-(4-Hydroxy-3-((2-(3-(5-(4-hydroxy-3-methoxybenzyl)-3-(4-methoxy-3-methyl phenyl)-6-oxo pyridazin-1(6H)-yl)propanoyl) hydrazono)methyl)benzyl)-1,2-dimethylimidazolium chloride (**9b**).* Obtained as a canary yellow solid (1.06 g, 77%); mp 196–197 °C. FT-IR (KBr) ν (cm^{-1}): 3430 (m, br), 3201 (m, sh), 1684 (s, sh), 1668 (s, sh), 1598 (s, sh), 1549 (m, sh), 1278 (s, sh), 1153 (s, sh), 763 (m, sh), 555 (m, sh). ^1H NMR (300 MHz, DMSO d_6): δ (ppm) 11.40 (s, 1H), 10.19 (s, 1H), 8.60 (s, 1H), 8.30 (s, 1H), 7.85–7.71 (m, 3H), 7.65 (d, J = 2.1 Hz, 2H), 7.30–7.17 (m, 1H), 7.10 (t, J = 7.6 Hz, 2H), 7.08–6.91 (m, 3H), 5.94 (s, 2H), 4.03 (s, 3H), 3.95 (s, 3H), 3.87 (s, 3H), 3.79 (s, 3H), 3.56 (s, 2H), 3.26 (t, J = 7.1 Hz, 2H), 2.84 (s, 3H), 2.67 (t, J = 7.2 Hz, 2H), 2.09 (s, 3H). ^{13}C NMR (151 MHz, DMSO d_6): δ (ppm) 169.21, 161.49, 160.62, 156.76, 151.82, 147.86, 146.26, 144.98, 143.08, 142.33, 136.51, 134.01, 131.96, 131.29, 128.60, 127.69, 125.85, 124.33, 123.13, 122.95, 121.47, 120.11, 119.75, 118.56, 117.88, 116.84, 115.08, 58.39, 57.09, 54.39, 50.45, 47.31, 43.68, 38.62, 32.36, 20.03 and 12.43. ESI-MS m/z: $[M - Cl^-]^+$ Calcd for $C_{37}H_{41}N_6O_7$ 681.76; Found 681.50. Anal. Calcd for $C_{37}H_{41}ClN_6O_7$ (M = 717.21 g/mol): C, 61.96; H, 5.76; N, 11.72; Found: C, 61.85; H, 5.76; N, 11.43.

*2.3.7.3. 1-(4-Hydroxy-3-((2-(3-(5-(4-hydroxy-3-methoxybenzyl)-3-(4-methoxy-3-methyl phenyl)-6-oxopyridazin-1(6H)-yl)propanoyl) hydrazono)methyl)benzyl)-triethylammonium chloride (**9c**).* Obtained as a yellowish-white solid (1.07 g, 74%); mp: 211–212 °C. FT-IR (KBr) ν (cm^{-1}): 3445 (m, br), 3222 (m, sh), 1689 (*vs*, sh), 1673 (s, sh), 1609 (s, sh), 1551 (m, sh), 1281 (s, sh), 767 (m, sh), 561 (m, sh). ^1H NMR (300 MHz, DMSO d_6): 10.74 (s, 1H), 10.08 (s, 1H), 9.03 (s, 1H), 7.81 (s, 1H), 7.61 (dd, J_1 = 2.5 Hz, J_2 = 10.0 Hz, 2H), 7.09–6.91 (m, 3H), 6.85–6.62 (m, 4H), 4.56 (s, 2H), 4.03 (s, 3H), 3.90 (s, 3H), 3.85 (s, 3H), 3.61 (s, 3H), 3.35 (t, J = 7.2 Hz, 2H), 3.16 (q, J = 7.0 Hz, 6H), 2.69 (t, J = 7.2 Hz, 2H), 2.19 (s, 3H), 1.35 (t, J = 6.8 Hz, 9H). ^{13}C NMR (151 MHz, DMSO d_6): δ (ppm) 169.56, 160.62, 158.74, 156.39, 148.86, 147.67, 143.33, 140.21, 136.32, 133.02, 131.87, 130.58, 128.60, 127.69, 125.85, 124.37, 123.13, 122.24, 120.11, 119.75, 118.45, 117.05, 115.84, 114.45, 66.42, 59.51, 57.15, 54.39, 48.31, 43.68, 32.26, 20.10 and 8.23. ESI-MS m/z: $[M - Cl^-]^+$ Calcd for $C_{38}H_{48}N_5O_7$ 686.82; Found 686.80. Anal. Calcd for $C_{38}H_{48}ClN_5O_7$ (M = 722.27 g/mol): C, 63.19; H, 6.70; N, 9.70; Found: C, 63.11; H, 6.71; N, 9.57.

*2.3.7.4. 1-(4-Hydroxy-3-((2-(3-(5-(4-hydroxy-3-methoxybenzyl)-3-(4-methoxy-3-methyl phenyl)-6-oxo pyridazin-1(6H)-yl)propanoyl) hydrazono)methyl)benzyl)-4-methoxypyridinium hexafluoro-phosphate (**9d**).* Obtained as a pale yellow powder (1.39 g, 83%); mp: 248–250 °C. FT-IR (KBr) ν (cm^{-1}): 3398 (m, br), 3211 (m, sh), 1683 (*vs*, sh), 1671 (s, sh), 1615 (s, sh), 1545 (m, sh), 1275 (s, sh), 1154 (s, sh), 841 (*vs*, sh), 738 (m, sh), 559 (m, sh). ^1H NMR (300 MHz, DMSO d_6): δ (ppm) 11.26 (s, 1H), 10.65 (s, 1H), 9.00 (s, 2H), 8.76 (s, 1H), 8.32 (s, 1H), 7.76 (dd, J = 7.2, 2.6 Hz, 3H), 7.68 (q, J = 4.1, 3.3 Hz, 2H), 7.48–7.29 (m, 6H), 6.98 (dd, J = 8.5, 1.7 Hz, 2H), 4.93 (s, 2H), 4.38 (s, 2H), 4.22 (s, 3H), 3.98 (s, 3H), 3.84 (s, 3H), 3.77 (s, 3H), 3.67 (s, 2H), 3.05 (t, J = 7.0 Hz, 2H), 2.59 (t, J = 7.0 Hz, 2H), 2.09 (s, 3H). ^{13}C NMR (75 MHz, DMSO d_6): δ (ppm) 177.82, 166.83, 161.39, 158.84, 153.52, 150.84, 149.57, 147.73, 146.54, 144.67, 142.30, 135.41, 132.80, 129.71, 129.58, 128.99, 128.48, 125.80, 124.49, 123.67, 121.09, 117.97, 117.43,

116.53, 115.38, 114.76, 114.44, 64.08, 58.29, 57.23, 55.51, 54.79, 50.49, 42.19, 31.75, 22.21. ^{31}P NMR (243 MHz, DMSO d_6) δ −144.19 (hept, $^2J_{PF}$ = 711.5 Hz). ^{19}F NMR (565 MHz, DMSO d_6): δ −70.13 (d, $^1J_{PF}$ = 711.3 Hz). ESI-MS *m/z*: [M – PF_6^-]$^+$ Calcd for $C_{38}H_{40}N_5O_8$ 694.75; Found 694.70. Anal. Calcd for $C_{38}H_{40}F_6N_5O_8P$ (M = 839.72 g/mol): C, 54.35; H, 4.80; N, 8.34; Found: C, 54.21; H, 4.91; N, 8.32.

2.4. Pharmacological part

2.4.1. Antimicrobial survey

2.4.1.1. Reagents. Dimethylformamide (DMF), Ciprofloxacin (Cip) ($C_{17}H_{18}FN_3O_3$, 331.34 g/mol), antibacterial drug, and amphotericin B (Am_B) ($C_{47}H_{73}NO_{17}$, 923.49 g/mol), antifungal drug, were obtained from Sigma Chemical Co. (St. Louis, MO, USA).

2.4.1.2. Culturing media. Nutrient Broth (NB): This medium was used for the growth of bacterial strains and it contains; peptone, beef extract, yeast extract, sodium chloride, distilled water (5:1:2:2:1000, W:W:W:W:W). The pH of NB was adjusted with buffer to 7.0 ± 0.2 and then sterilized by autoclaving at 121 °C for 15 min.

Sabouraud dextrose agar (SDA): This medium was used for growth and biofilm-producing of *C. albicans*. It contains; dextrose, peptone, agar, distilled water (40:10:20:1000, W:W:W:W). The pH of SDA was adjusted with buffer to 5.6 ± 0.1 and then sterilized by autoclaving at 121 °C for 15 min.

2.4.1.3. Inoculum stocks. Bacterial strains used in this study were obtained from national organization for drug control and research (NODCAR), Cairo, Egypt. The different strains are *Staphylococcus aureus* (*S. aureus*, ATCC-29737), *Bacillus subtilus* (*B. subtilus*, NCTC-1040) as gram-positive bacteria, *Escherichia coli* (*E. coli*, ATCC-10536), Pseudomonas aeruginosa (*P. aeruginosa*, ATCC-27853) as gram-negative pathogenic bacteria and as well *Candida albicans* (*C. albicans*, RCMB 05038) as a fungal pathogen. Stock cultures of bacterial strains were grown aerobically on NB agar slants (Hi-Media) while *C. albicans*, fungal strain, was grown on NB and SDA, respectively, at 37 °C and then maintained at 4 °C. After 24 h of incubation, bacterial and fungal suspension were diluted with sterilized physiological solution and the turbidity of each suspension was adjusted to match 0.1 optical density at 600 nm (≈10^8 CFU/mL) (CFU = Colony Forming Units) using spectronic21 (Bauch and Lomb, New York, USA) and were used as inoculum for all experiments.

2.4.1.4. Antimicrobial performance. Antibacterial susceptibility of the bacterial strains was carried out by plates assay method, in briefly, the Mueller-Hinton agar (MHA) plates were inoculated with the 0.1 mL of fresh culture having (10^8 CFU/mL) of each test organism by dipping a sterile cotton swab into the suspension. The swab was then streaked over the entire surface of the MH medium three times, rotating the plate approximately 60° after each application to ensure an even distribution of the inoculum. After that petri dishes are placed in the refrigerator at 4 °C or at room temperature for 1 h for diffusion. The wells (6 mm) were made in the seeded agar using sterile cork borer, then 50 μL of the concentration 5 mg/mL of the tested sample was added into the wells and allowed to diffuse. The plates were incubated at 37 °C for 24 h, after that the zone of inhibition (ZoI) that observed around each disc was measured with a transparent ruler in mm. Standard drug (Cip) disc (5 mg/disc) are placed on the fourth compartment of the plate with the help of sterile forceps as a positive control while DMF was used as negative control. Observe the ZoI produced by different samples. Measure it using a scale and record the average of two diameters of each ZoI. According to Ciobanu et al., ZoI in mm considers being qualitative screening [30] for antimicrobial activity of material. On the other hand, the antifungal screening of new compounds against *C. albicans* was carried out by disc diffusion method, in brief; SDA medium was prepared and transferred into sterile petri plates aseptically (thickness of 5–6 mm). The plates were allowed to dry at room temperature. The plates were inverted to prevent condensate falling on the agar surface. The layers of the medium should be uniform in thickness which is done by placing the plates on a leveled surface. Standardized fungal inoculums (2×10^6 CFU/mL) of *C. albicans* was applied to the plates and speeded uniformly over the surface of medium by using a sterile non-absorbent cotton swab and finally the swab was passed around the edge of the medium. The inoculated plates were closed with the lid and allowed to dry at room temperature. The sample impregnated discs (5 mg/disc) and DMF was used as negative control, standard Am_B 6 mg/disc was placed on the inoculated agar medium as positive control. All petri plates were incubated at 27–28 °C for 48 h.

2.4.1.5. Determination of MIC and MBC. As rational parameters for the antibacterial efficacy, the minimal inhibitory concentration (MIC) and minimal bactericidal concentration (MBC) of the new compounds against the panel of tested bacterial strains were determined using the macro-dilution broth susceptibility test. Freshly prepared MH broth was used as diluents in the macro-dilution method test [24b] A serial dilution of each target compound was prepared within a desired range (0.1–50 μg/mL). One milliliter of the stock cultures was then inoculated and tubes were incubated at 37 °C for 24 h, control tubes without any addition were assayed simultaneously. MIC was examined visually, by checking the turbidity of the tubes. Furthermore the tubes having lesser concentration than MIC level were inoculated on MHA plate for MBC determination.

3. Theoretical and computational analysis

The theoretical calculation of the molecular structure by using different computational methods allows the exploration of molecules through the use of a computer in cases when an actual laboratory investigation may be inappropriate, impractical, or impossible.

3.1. Hydrophobicity (lipophilicity)

Molecular hydrophobicity (lipophilicity), usually quantified as log P (the logarithm of 1-octanol/water partition coefficient), plays a key role in assessing the biological features relevant to pharmacological agent action, such as lipid solubility, tissue diffusion, binding receptor, cellular uptake, bioavailability and pharmacokinetic [31]. Among the most useful computational methods for estimating log P values, ClogP [32] is of the most widely used method. The values of ClogP were calculated using ChemDraw Ultra 12.0 software integrated with Cambridge Software (Cambridge Soft Corporation). The values of ClogP were depicted in Table 1.

3.2. Molecular docking study

Molecular docking of target compounds (**8a**, **9b**) into the proteins compromising the crystal structure of β-ketoacyl-acyl carrier protein synthase, FabH, (PDB code 1HNJ) as promising target of *E. coli* strain [33] was carried out using the AutoDock software package (version 4.0) as implemented through the graphical user interface AutoDockTools (ADT) [34]. Prior to the calculations, the inter-structure water and ligand molecules were removed from the X-ray structure (Fig. S1). The whole docking process was done using Molecular Operating Environment [35] and addition of atomic charges was done through AutoDock Tools. The standard parameter settings were applied. High-scoring binding poses were selected on the basis of visual inspection.

4. Results and discussion

4.1. Synthesis protocol

The green key starting materials vanillyl ionic liquids (Val-ILs) (**2a**–**d**) were synthesized *via* an efficient chloromethylation of vanillin using paraformaldehyde/HCl_{aq} as a chloromethylating mixture in presence

Table 1
ClogP and MIC/MBC (μg/mL) values for compounds **8a–c**, **9a–d** and clinical drugs.[a]

Compd.	ClogP	Gram-positive bacteria				Gram-negative bacteria			
		S. aureus ATCC29737		*B. subtilis* CECT498		*E. coli* ATCC25922		*P. aeruginosa* ATCC27853	
		MIC	MBC	MIC	MBC	MIC	MBC	MIC	MBC
8a	5.04	4.25 ± 0.3	4.50 ± 0.3	2.98 ± 0.1	3.03 ± 0.3	9.95 ± 0.2	10.50 ± 0.3	13.50 ± 0.1	14.12 ± 0.4
8b	3.78	–	–	20.50 ± 0.3	21.60 ± 0.3	20.13 ± 0.9	20.10 ± 0.8	–	–
8c	3.21	20.50 ± 0.7	21.30 ± 0.8	>50	>50	–	–	–	–
9a	0.13	16.40 ± 1.2	17.95 ± 1.1	21.80 ± 0.9	22.75 ± 1.0	30.15 ± 1.4	31.13 ± 1.3	25.30 ± 1.2	26.20 ± 1.3
9b	−1.83	2.96 ± 0.3	3.05 ± 0.3	5.96 ± 0.1	6.11 ± 0.1	13.05 ± 0.9	13.25 ± 0.8	1.98 ± 0.1	2.18 ± 0.1
9c	0.24	15.75 ± 0.9	16.70 ± 0.8	20.40 ± 1.1	21.30 ± 1.0	–	–	22.85 ± 0.9	23.75 ± 1.0
9d	−0.45	13.50 ± 0.8	14.65 ± 0.8	16.75 ± 0.7	17.75 ± 0.6	24.70 ± 1.5	25.15 ± 1.5	22.75 ± 1.2	23.70 ± 1.2
Cip	−0.73	5.75 ± 0.2	6.22 ± 0.2	5.53 ± 0.1	5.55 ± 0.1	5.53 ± 0.2	5.55 ± 0.2	10.22 ± 1.7	11.14 ± 1.7

[a] ClogP = molecular hydrophobicity (the logarithm of 1-octanol/water partition coefficient); MIC = minimal inhibitory concentration (the lowest concentration which resulted in maintenance or reduction of inoculum viability); MBC = minimal bactericidal concentration (the lowest concentration of an anti-microbial agent that will restrict the growth of the organism when subcultured into antibiotic-free media).

catalytic amount of $ZnCl_2$ under a stream of gaseous HCl to obtain chloromethyl-vanillin (CMVal) which used as an efficient alkylating agent for quaternization of organonitrogen compounds such as 4-methoxypyridine (4-MeOPy), 1,2-dimethylimidazole (1,2-Me_2Im) and triethylamine (Et_3N) to yield Val-ILs (**2a–c**) in satisfactory yields. Anion metathesis of **2a** with hexafluorophosphoric acid ($HPF_{6(aq)}$) afford the corresponding hexafluorophosphate salt (**2d**) (Scheme 1A). In other synthetic route, 6-anisyl-3(2H)-pyridazinone (**4**) was synthesized starting from 2-methylanisole through a Friedel–Craft acylation of *o*-methyl anisole with succinic anhydride in the presence of anhydrous aluminium chloride (a Lewis acid catalyst) to yield β-substituted benzoyl propionic acid (**3**) which subjected to cyclocondensation reaction with hydrazine hydrate resulted in the formation of dihydropyridazinone (**4**). Thereafter, Knoevenagel condensation of 4,5-dihydropyridazinone (**4**) with vanillin in the presence of KOH afford the corresponding 4-vanillylpyridazinone derivative (**5**) (Scheme 1B). Subsequent alkylation of 4-vanillylpyridazinone derivative (**5**) with methyl 3-bromopropionate gave the corresponding ester (**6**), which was either transformed into the corresponding carboxylic acid (**7a**) by alkaline hydrolysis under standard conditions or converted into the corresponding hydrazide (**7b**) *via* hydrazinolysis reaction conditions (see Scheme 2). Activation of the acid (**7a**) with ethyl chloroformate in the presence of triethylamine in THF led to the formation of an active mixed anhydride intermediate, which was easily transformed into the final amides (**8a–c**), in good yields, by treatment with appropriate aryl amines.

On the other hand, the green Val-ILs (**2a–d**) were used to functionalize hydrazide (**7b**) *via* facile condensation under reflux conditions affording the corresponding IL-based hydrazones (**9a–d**) in good yields, as depicted in Scheme 2.

4.2. Structural characterizations

All newly synthesized compounds were prepared in convinced yields and exhibited satisfactory CHN elemental analyses which are in fully agreement with their proposed structural formulas (see the Experimental section).

The main feature of electron impact mass spectra (EI-MS) of new pyridazinone-propanamides (**8a–c**) is the notice of predominant peaks at m/z = 567.50, 529.50 and 559.60 corresponding to the molecular ion peak $[M]^+$ of **8a–c**, respectively, a molecular mass signature. However, the positive mode electrospray ionization mass spectra (ESI-MS) of new IL-based pyridazinone-hydrazones derivatives (**9a–d**) exhibited dominant peaks at m/z = 694.70, 681.750, 686.80 and 694.70 assignable to a singly-charged cation produced *via* departure of the anion from their parent molecule, $[M - X^-]^+$ (X = Cl or PF_6).

FTIR spectra offer primary spectral markers for proofing the successful formation of new pyridazinone-propanamides (**8a–c**) as revealed

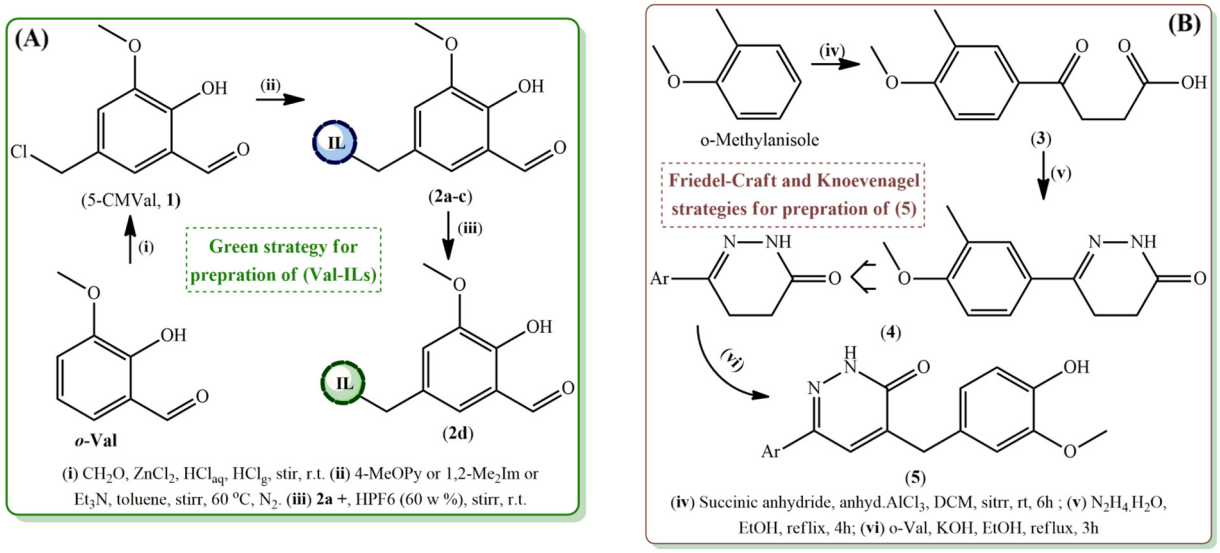

Scheme 1. Schematic protocol for preparation of key starting materials: (A) Green vanillyl ionic liquids (Val-ILs) (**2a–d**); (B) Knoevenagel condensation product (**5**).

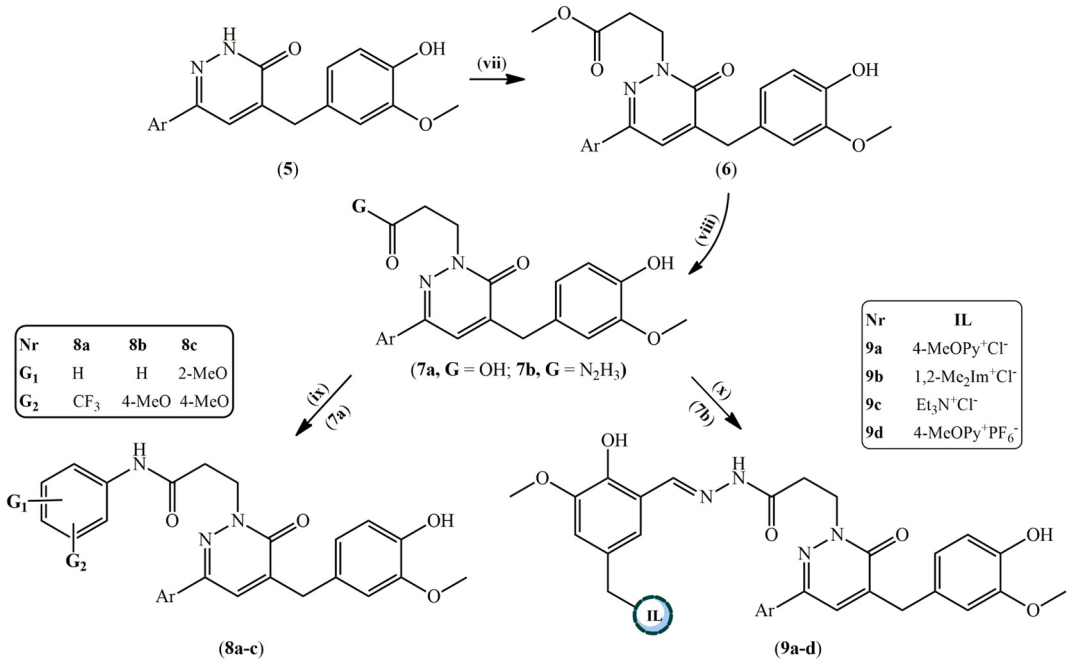

Scheme 2. Schematic diagram for preparation of pyridazinone-based propanamides (**8a–c**) and amphiphilic hydrazones (**9a–d**).

from their FTIR signatures at 3298–3210 cm^{-1} and 1676–1665 cm^{-1} characteristic for the stretching vibrations of N—H and C═O moieties, respectively, involved in amide-bond segment. On the other hand, infrared spectral detection of 4-vanillylpyridazinone propionylhydrazide (**7b**) fragment in the new IL-based pyridazinone compounds (**9a–d**) may be confirmed for the observation of stretches around 3445 and 3194 cm^{-1}, characteristic for the vibrational modes of O—H (vanillyl) and N—H (hydrazide), respectively, along with maxima at *ca.* 1689 and 1665 cm^{-1} assignable to C═O of pyridazinone and hydrazide, respectively. Moreover, anchoring of hydrazide (**7b**) to Val-ILs (**2a–d**) can be detected from the growth of new maxima in the spectra of **9a–d** around 1600 cm^{-1}, characteristic for the azomethine (—CH═N—) stretching vibration (Fig. 1), coupled with the notice of three predominate stretches at the range of 1556–1545 cm^{-1} for C═N stretching vibration; 565–555 cm^{-1} for Het-N^+X^- vibration and 767–738 cm^{-1} attributable for the Im/Py bending vibration, which are characteristic for the IL terminal.

Diagnostically, $^1H/^{13}C$ NMR spectra (Figs. S2–S15, Supplementary data) provides the second and strong spectral evidence for the successful formation of pyridazinone-propanamides (**8a–c**) as revealed from the emergence of two singlets at ~11.00 ppm (due to Ar–O**H**) and ~8.00 ppm (due to CO–N**H**) in their ^1H NMR spectra coupled with two characteristic peaks observed around 150 ppm (due to **Ar**–O) and 173 ppm (due to carboxamide group (**C**O–NH)) in their ^{13}C NMR spectra. Additionally, ^1H NMR spectral markers including two characteristic singlets ~12.00/~11.00 ppm (assigned as Ar–O**H**) and at *ca.* 9.00/8.50 ppm which can assigned as N–H and azomethinic protons, respectively, provide a splitting pattern which is in fully agreement with the successful preparation of IL-based pyridazinone (**9a–d**).

4.3. Pharmacological studies

4.3.1. Antibacterial activity

The *in vitro* antibacterial screening of new pyridazinone derivatives in comparison to ciprofloxacin (Cip) as a standard antibiotic was assessed against four common pathogenic bacteria *S. aureus* (ATCC29737) and *B. subtilus* (CECT498) delegate for gram-positive (G^+) bacteria, as well as *E. coli* (ATCC25922) and *P. aeruginosa* (ATCC27853) delegate for gram-negative (G^-) bacteria. Preliminary *in vitro* antibacterial survey (Fig. 2) demonstrated that the majority of the tested compounds could effectively curb the growth of bacterial strains along with broad-spectrum antibacterial efficacy as revealed from the collected zone of inhibition (ZoI) and the minimal inhibitory concentration (MIC) and minimal bactericidal concentration (MBC) values which were depicted in Fig. 2 and Table 1, respectively. Against G^+ bacteria *S. aureus*, compounds **9b** and **8a** ($MIC/MBC_{S.\ aureus}$ = 2.96/3.05 and 4.25/4.50 μg/mL, respectively) were found to be the most effective and have potency exceed or comparable to that of positive control (Cip) ($MIC/MBC_{S.\ aureus}$ = 5.75/6.22 μg/mL). On the other hand, against the G^+ bacteria *P. aeruginosa*, compound **9b** ($MIC/MBC_{P.\ aeruginosa}$ = 1.98/2.18 μg/mL) exhibited remarkable excellent activity as compared to the clinical drug Cip ($MIC/MBC_{P.\ aeruginosa}$ = 10.22/11.14 μg/mL) as well as to other members of the series.

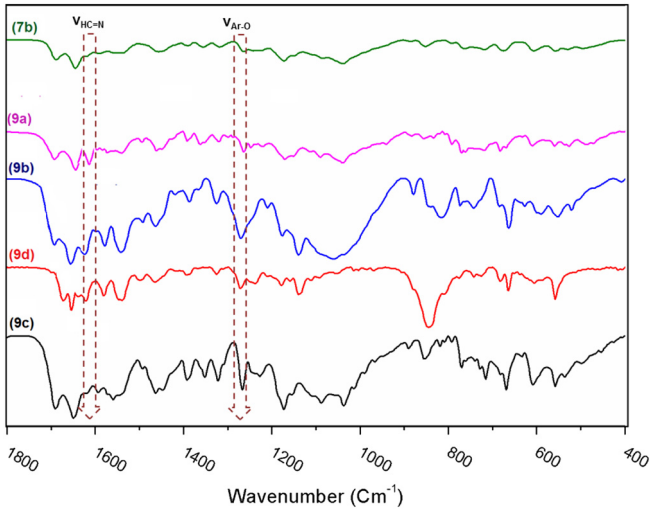

Fig. 1. Partial FTIR patterns for comparison of the azomethine (H—C═N) stretching vibrations and splitting patterns of hydrazide (**7b**) with IL-based pyridazinone-hydrazones derivatives (**9a–d**). H—C═N stretch around 1660 cm^{-1}; aryl–O vibration bands at *ca.* 1280 cm^{-1}.

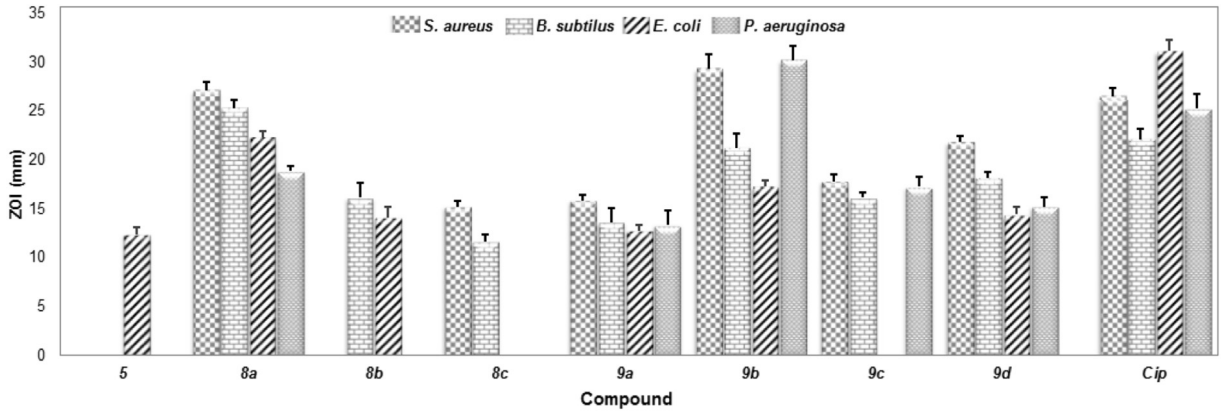

Fig. 2. Graph of ZoI (mm) for new pyridazinone derivatives against different bacterial species. Conditions for measurement of ZoI (see Experimental section).

The compounds **8c** and **9c** are inert toward *E. coli* while showed moderate activity against G^+ bacteria *S. aureus* ($MIC/MBC_{S.\ aureus}$ = 15.75/16.70 and 20.50/21.30 μg/mL, respectively). Compound **8a** ($MIC/MBC_{E.\ coli}$ = 10.95/11.50 μg/mL) is the most active member against *E. coli* in comparison with the other compounds. Compounds **9a**, **9c** and **9a** showed moderate to high broad-spectrum activity as compared to **8a** and **8b** against the whole panel of bacterial species.

4.3.2. Anticandidal assays

The *in vitro* anticandidal evaluation revealed a wide range of activities for screened pyridazinone derivatives: from somewhat active to highly active through moderately active members (Fig. 3). For example, the parent vanillylpyridazinone (**5**) exhibited somewhat activity against *C. albicans* CECT1394. Among the series of propanamides analogues (**8a–c**), compound **8a** exerted the best efficacy in inhibiting the growth of *C. albicans* strain (MIC/MBC = 1.05/1.05 μg/mL) which exceed that of antifungal control amphotericin B (Am_B) (MIC/MBC = 10.20/10.20 μg/mL), while, **8b** and **8c** showed lower anticandidal action in comparison to **8a** and clinical antifungal drug (Am_B) as revealed from ZoI and MIC/MBC values. In the other series of IL-based propionylhydrazide (**9a–d**), **9a** exhibited excellent anticandidal activity (MIC/MBC = 0.50/0.50 μg/mL) which was 20 times more active than reference drug, Am_B (MIC/MBC = 10.20/10.20 μg/mL).

4.3.3. Structure–activity relationship (SAR)

Pharmacological results demonstrated the importance of the substitution pattern of the N2-arm endured by the vanillylpyridazinone scaffold in tuning the antimicrobial action for the target compounds. It emerged that the amide and hydrazonoyl segments, substituents and ionic liquid terminals were found to be responsible for variation in activity. Generally, anchoring of aryl propanamides compartments in (**8a–c**) or Val-ILs to vanillyl-pyridazinone in ILs-based propionylhydrazide (**9a–d**) is significantly enhanced the antimicrobial efficacy with higher susceptibility of tested microbial species toward the IL-based propionylhydrazide (**9a–d**) more than propanamides (**8a–c**). Among vanillyl-pyridazinone propanamides series (**8a–c**), compound **8a** with 4-(trifluoromethyl)phenyl group exerted extremely high activities against all tested strains with anti-*B. subtilus* activity (MIC/MBC = 2.98/3.03 μg/mL) 1.5-fold and ~3.5-fold higher than antistaphylococcal and anti-*E. coli* activities (MIC/MBC = 4.25/4.50 and 9.95/10.50 μg/mL, respectively). A significant negative-shift in antibacterial profile was observed against entire range of bacterial strains on substituting 4-trifluoromethy group with 4-methoxy in **8b** or 2,4-dimethoxy groups in **8c**. On replacing the propanamide segment with propionylhydrazide, **9a–d**, having Val-ILs compartment a remarkable enhancement in the antimicrobial performance against the entire range of bacterial strains was observed. Particularly, dimethylimidazolium-based propionylhydrazide (**9b**) which is at the forefront of all members in its effect against all microbial species as revealed from ZoI and MIC/MBC (1.98–13.15/2.18–13.07 μg/mL) values. Noteworthy, compound **9b** exhibited higher activity in comparison to the clinical drug, Cip. This remarkable extremely high biopotency of **9b** and **8a** may be ascribed for the anchoring of diverse antimicrobial pharmacophores to the vanillylpyridazinone scaffold in their structures (see Fig. 4) which exerts overall synergistic microbiological effects. The prominent pharmacophores in these compounds may be categorized into three main groups: (i) Hydrophobic pharmacophores such as multiple methyl groups which play a crucial role in penetration of the lipophilic core of a bacterial cell membrane. (ii) Hydrogen-bonding donor/acceptor (HBD/HBA) sites are important for hydrogen bonding interactions with DNA nucleobases and subsequently disordering its function and/or its formation.

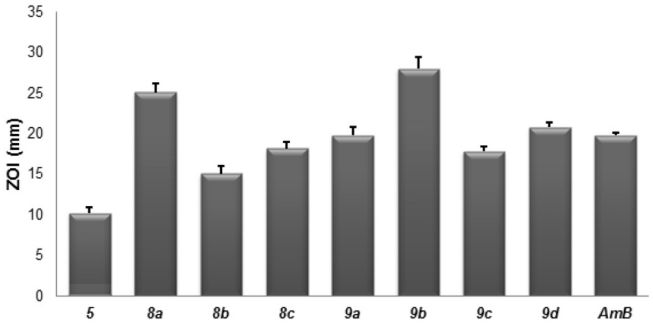

Fig. 3. Graph of ZoI (mm) for anticandidal activities of new pyridazinone derivatives. Disc diffusion method was used measurement of ZoI for anticandidal agents (see the Experimental section).

4.3.4. Effect of ClogP values on antimicrobial activity

Molecular hydrophobicity (lipophilicity) is one of the most key features in predicting the pharmacological properties for the clinical trials [36]. The ClogP computational method was the first simply implemented method to predict the lipophilicity of molecule through stimulation of ClogP values which are in strong relevance with the lipophilicity and subsequently the bioactivity of target molecules. The stimulated 1-octanol/water partition coefficients (ClogP) for the most potent pyridazinone derivatives were collected in Table 1. The obtained data demonstrated that compounds with lower ClogP values exhibited enhanced antimicrobial activities. For instance, compound **9b** with lowest ClogP (−1.83) exerted the best antimicrobial action as previously discussed. However, in case of propanamides analogues (**8a–c**) an increasing of ClogP value result in an enhancement of the antimicrobial activities. For example compound **8a** with ClogP (5.04) have higher antimicrobial efficacy than clinical drugs. This might be explained by the possibility that higher lipophilic character was favorable for being

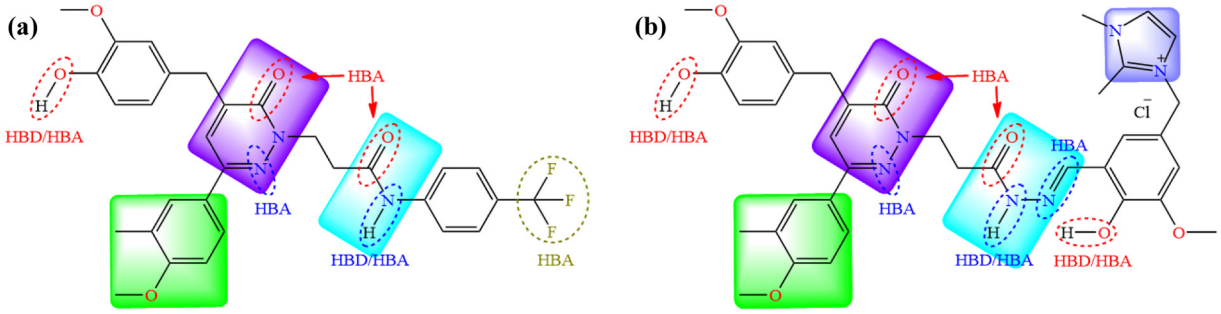

Fig. 4. Schematic graphs for: (a, b) All possible bioactive pharmacophores in **8a** and **9b,** respectively. HBD/HBA = H-bonding donor/acceptor sites. Highlighted common antimicrobial pharmacophores exert their pharmacological effects through different modes of actions.

delivered through the *lipophilic layer* of microbial cell wall, and manifested the significant role of suitable lipophilicity in drug design.

4.4. Computational studies

4.4.1. Hydrophilicity/lipophilicity balance

The biocompatibility and antimicrobial performance of the biological molecule is strongly correlates to its hydrophilicity which may be tuned refining of its molecular structure. Thus, the simulation study of the lipophilicity character of the compounds **8a** and **9b** was carried out and the obtained data was collected in Fig. 5 which showed strong lipophilic profile of the terminals coupled with some neutral behavior in the middle along with an infinitesimal hydrophilicity character for compound **8a**. While compound **9b** exhibited strong lipophilic character associated with one terminal with some neutral behavior in the middle and strong hydrophilicity for the other terminal. As a result, it would be expected that **9b** is more potent than **8a** as antimicrobial agent due to its enhanced hydrophilicity.

4.5. Molecular docking study

In an effort to investigate the possible mechanism by which the title compounds 8a and 9b can induce antibacterial activity easier to understand and guide further SAR studies, the molecular docking of all the compounds with *E. coli* FabH was performed on the binding model based on the *E. coli* FabH-CoA complex structure (1HNJ.pdb) [37], The binding modes of potent inhibitor **8a** and **9b** with 1HNJ were depicted in Fig. 6. As depicted in Fig. 6a,c, the binding model of **8a** revealed an interested **8a**-1HNJ interaction *via* two hydrogen bonds, two aromatic π-stacking modes, and one hydrophobic interaction. The intermolecular H-bonds are formed by association of Gly209 and Arg151 with the NH of amide fragment and oxygen atom of methoxy group of anisyl ring with distances of 1.59 Å and 3.34 Å, respectively. Further, the benzyl moiety forms two aromatic stacking interactions with the two Arg36 (distance: 3.21 Å and 5.14 Å) and Arg249 (distance: 3.21 Å and 5.18 Å). Moreover, the triflurophenyl ring was accommodated in big hydrophobic pocket formed of Phe213, Ala246, Met207, Val212, and Phe304 residues enhancing the binding action between target enzyme and compound **8a**.

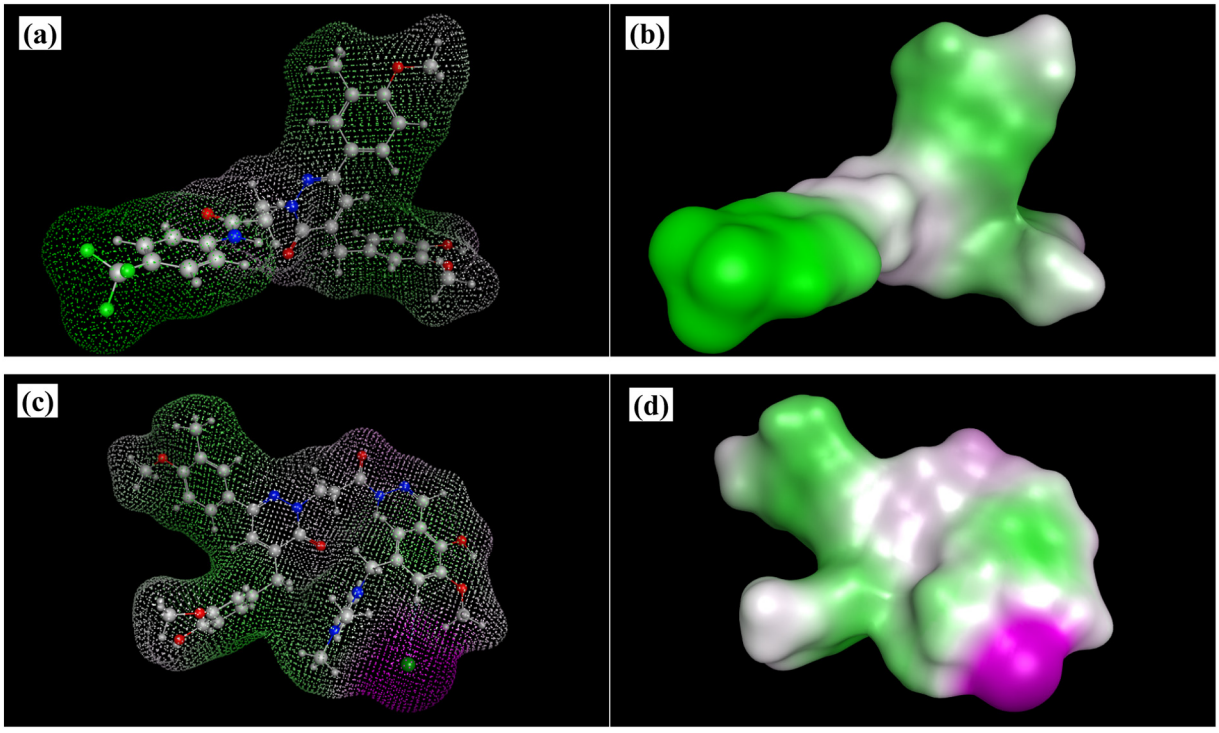

Fig. 5. The lipophilic and hydrophilic character of: (a,b) compound **8a**; (c,d) compound **9b** where (red = hydrophilic; white = neutral; green = lipophilic). (For interpretation of the references to color in this figure legend, the reader is referred to the web version of this article.)

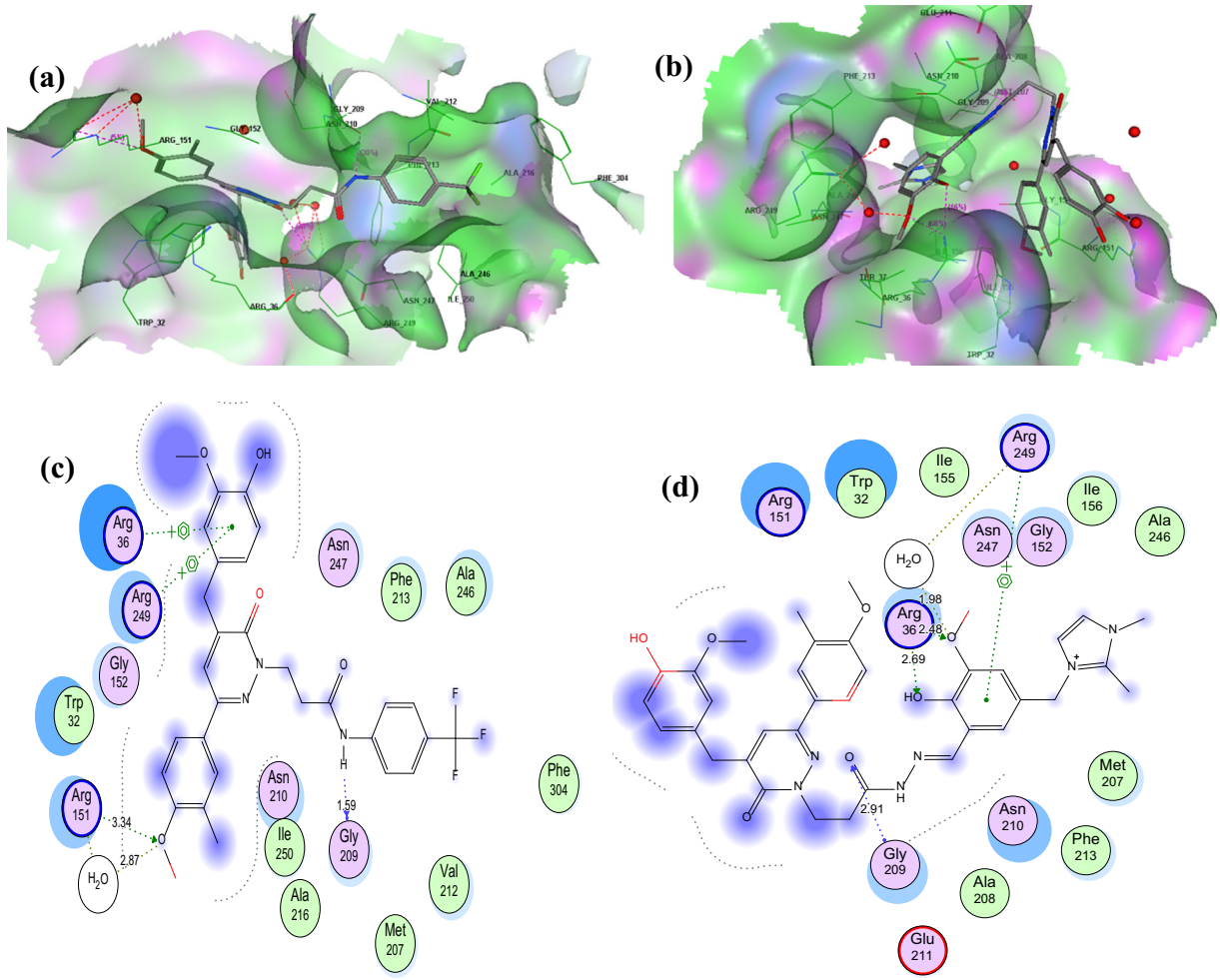

Fig. 6. (a,b) 3D model of the electrostatic map and interaction between compound **8a** and **9b** in the 1HNJ bonding site; (c,d) 2D molecular docking modeling of compound **8a** and **9b** with 1HNJ. Ball and stick, showing hydrogen bonds (green dotted arrows) and π-stacking interactions (green dotted lines) involving flexible docking into FabH. (For interpretation of the references to color in this figure legend, the reader is referred to the web version of this article.)

Interestingly, compound **9b** exhibits more attracted bonding pattern Fig. 6b,d *via* three hydrogen bonds together with one π-stacking aromatic interaction. A remarkable hydrogen bond is formed by the oxygen atom of C═O belongs to the hydrazinocarbonyl moiety and Gly209 with distance of 2.91 Å. As well, the Arg36 residue forms two hydrogen bonds with o-vanilinyl —OH and —OCH_3 groups by distances of 2.69 Å and 1.98 Å, respectively. Furthermore, small hydrophobic groove tolerates the terminal imidazolinium cation by Met207, Ala246, and Phe213 residues. The electrostatic maps are presented for the two compounds in the binding pocket showing the polar and hydrophobic areas with the contacts preferences.

The lower binding energy for **8a** (−14.4 kcal/mol) as compared with that of **9b** (−12.5 kcal/mol), Table 2, coupled with its binding pattern pronounced the good binding affinity for *E. coli* FabH, revealed that the accommodation of compound **8a** is more better than **9b** due to its lower surface area and higher lipophilicity parameters which are significantly affected the interactions of antimicrobial agent with the target enzyme, FabH. In conclusion, compound **8a** is more efficacious than **9b** toward the target receptor and consequently exhibited more potent anti-*E. coli* activity which in fully agreement with our obtained antimicrobial data. Moreover, from this binding model, it could be concluded that H-bonding, π-stacking and hydrophobic interactions may be considered responsible for the mode of antimicrobial action for compound **8a** and its analogues. However, H-bonding, π-stacking and π–cation interactions may offer rational explanation for the mode of antimicrobial action for compound **9b** and its analogues.

5. Conclusion

In conclusion, a novel series of pyridazinone-vanillyl conjugates with a neutral N(2)-arm of arylpropanamides (**8a–c**) or amphiphilic arm of Val-ILs (**9a–d**) have been successfully prepared starting from commercially available 2-methylanisole and vanillin. The structures of new compounds were elucidated based upon elemental and spectral analysis (FTIR, ^{1}H NMR, ^{13}C NMR, ^{31}P NMR, ^{19}F NMR, EI-MS and ESI-MS). These new pyridazinone-based antibiotic candidates exhibited remarkable and broad-spectrum antimicrobial efficacy with low MIC/MBC values. Among these of pyridazinone-vanillyl conjugates, compound **9b** bearing amphiphilic dimethylimidazolium group is at the

Table 2
Molecular properties of target compounds.

Parameter[a]	8a	9b
MW	567.56	681.77
Log P	5.98	4.29
TPSA	100.46	151.1
HBD	2	3
HBA	6	9
BE (kcal/mol)	−14.4	−12.5

[a] MW = molecular weight; log p = a measure of hydrophobicity; TPSA = total polar surface area, a measure of hyrophilicity (polarity); HBD = hydrogen bond donors; HBA = acceptors, a measure of possibility to interact tightly with the targets; BE = binding energy.

forefront of all new compounds in its effect against all bacterial strains as revealed from its ZoI and MIC/MBC values. For instance, **9b** (with amphiphilic arm) (MIC/MBC = 3.96/3.98 μg/mL) is 2.3-fold more potent than **8a** (with neutral arm) (MIC/MBC = 8.95/8.99 μg/mL) as antistaphylococcal agent. Combined analysis of biological data along with the *in Silico* derived parameters demonstrated the importance of the chemical nature of the N(2)-arm in tuning the antibacterial potency of the target compound. The molecular docking study revealed that **8a** was found more effective in binding to the active site of *E. coli* FabH in comparison to **9b**.

Conflict of interest

The authors declare no conflict of interest.

Acknowledgments

We would like to thank Dr. Hany E. A. Ahmed, College of Pharmacy, Taibah University, Saudi Arabia and Prof. Dr. Adel S. Orabi, Faculty of Science, Suez Canal University, Egypt, for their generous supporting this work.

Appendix B. Supplementary data

Supplementary data (experimental details on materials and instrumentation, structure of *E. coli* FabH (PDB code: 1HNJ)) associated with this article are available with the article through the journal Web site, at https://doi.org/10.1016/j.molliq.2018.03.022.

References

[1] (a) P.N. Batalha, A.T.P.C. Gomes, L.S.M. Forezi, L. Costa, M.C.B.V. de Souza, F.C.S. Boechat, V.F. Ferreira, A. Almeida, M.A.F. Faustino, M.G.P.M. Neves, Synthesis of new porphyrin/4-quinolone conjugates and evaluation of their efficiency in the photoinactivation of *Staphylococcus aureus*, RSC Adv. 5 (87) (2015) 71228–71239;
(b) X. Wang, O.S. Wolfbeis, Fiber-optic chemical sensors and biosensors, Anal. Chem. 85 (2) (2013) 487–508.
[2] Y. Zhao, Y. Tian, Y. Cui, W. Liu, W. Ma, X. Jiang, Small molecule-capped gold nanoparticles as potent antibacterial agents that target gram-negative bacteria, J. Am. Chem. Soc. 132 (35) (2010) 12349–12356.
[3] M.-P. Mingeot-Leclercq, J.-L. Decout, Bacterial lipid membranes as promising targets to fight antimicrobial resistance, molecular foundations and illustration through the renewal of aminoglycoside antibiotics and emergence of amphiphilic aminoglycosides, Med. Chem. Commun. 7 (4) (2016) 586–611.
[4] J. Chen, F. Wang, Q. Liu, J. Du, Antibacterial polymeric nanostructures for biomedical applications, Chem. Commun. 50 (93) (2014) 14482–14493.
[5] J.G. Longo, I. Verde, M.E. Castro, Pyridazine derivatives. XI: antihypertensive activity of 3 hydrazinocycloheptyl[1,2-c]pyridazine and its hydrazone derivatives, J. Pharm. Sci. 82 (1993) 286–290.
[6] W. Malinka, A. Redzicka, O. Lozach, New derivatives of pyrrolo [3,4-d] pyridazinone and their anticancer effects, Il Farmaco 59 (2004) 457–462.
[7] D.G.H. Livermone, R.C. Bethell, N. Cammack, Synthesis and anti-HIV-1 activity of a series of imidazo [1,5-b] pyridazines, J. Med. Chem. 36 (1993) 3784–3794.
[8] S. Demirayak, A.C. Karaburun, R. Beis, Some pyrrole substituted aryl pyridazinone and phthalazinone derivatives and their antihypertensive activities, Eur. J. Med. Chem. 39 (2004) 1089–1095.
[9] A.A. Siddiqui, S.M. Wani, Synthesis and hypotensive activity of some 6-(substituted aryl)-4-methyl-2, 3 dihydropyridazin-3-ones, Indian J. Chem. 43B (2004) 1574–1579.
[10] A. Coelho, E. Sotelo, E. Ravina, Pyridazine derivatives. Part 33: Sonogashira approaches in the synthesis of 5-substituted-6-phenyl-3 (2H)-pyridazinones, Tetrahedron 59 (2003) 2477–2484.
[11] C. Rubat, P. Coudert, B. Refouvelet, P. Tronche, P. Bastide, Anticonvulsant activity of 3-oxo-5-substituted benzylidene-6-methyl-(4H)-2-pyridazinylacetamides and 2-pyridazinylacetylhydrazides, Chem. Pharm. Bull. 38 (11) (1990) 3009–3013.
[12] A. Monge, P. Parrado, M. Font, E.F. Alvarez, Selective thromboxane synthetase inhibitors and antihypertensive agents. New derivatives of 4-hydrazino-5H-pyridazino[4,5-b]indole, 4-hydrazinotriazino[4,5-a]indole, and related compounds, J. Med. Chem. 30 (6) (1987) 1029–1035.
[13] I. Sircar, R.E. Weishaar, D. Kobylarz, W.H. Moos, J.A. Bristol, Inhibition of separated forms of cyclic nucleotide phosphodiesterase from Guinea pig cardiac muscle by 4,5-dihydro-6-[4-(1H-imidazol-1-yl)phenyl]-3(2H)-pyridazinones and related compounds. Structure-activity relationships and correlation with in vivo positive inotropic activity, J. Med. Chem. 30 (1987) 1955–1962.
[14] A. Akahane, H. Katayama, T. Mitsunaga, Discovery of 6-Oxo-3-(2-phenylpyrazolo[1,5-*a*]pyridin-3-yl)-1(6H)-pyridazinebutanoic acid (FK 838): a novel non-xanthine adenosine A1 receptor antagonist with potent diuretic activity, J. Med. Chem. 42 (1999) 779–783.
[15] E. Sotelo, A. Coelho, E. Ravina, Pyridazines. Part 34: retro-ene-assisted palladium-catalyzed synthesis of 4, 5-disubstituted-3 (2H)-pyridazinones, Tetrahedron Lett. 44 (2003) 4459–4462.
[16] A.A. Siddiqui, S.R. Ahmad, S.A. Hussain, Synthesis and biological evaluation of some pyridazinone derivatives, Acta Pol. Pharm. 64 (2) (2008) 223–228.
[17] A. Siddiqui, A. Ashok, S.M. Wani, Synthesis and anti-inflammatory activity of 6-(substituted aryl)-2,3,4,5-tetrahydro-3-thiopyridazinones, Indian J. Heterocycl. Chem. 13 (2004) 257–260.
[18] K. Abouzid, M.A. Hakeem, O. Khalil, Y. Maklad, Pyridazinone derivatives: Design, synthesis, and in vitro vasorelaxant activity, Bioorg. Med. Chem. 16 (2008) 382–389.
[19] D.W. Combs, M.S. Rampulla, S.C. Bell, D.H. Klaubert, A.J. Tobia, R. Falotico, B. Haertlein, C.L. Weiss, J.B. Moore, 6-Benzoxazinylpyridazin-3-ones: potent, long-acting positive inotrope and peripheral vasodilator agents, J. Med. Chem. 22 (1990) 380–386.
[20] D.W. Robertson, N.D. Jones, J.H. Krushinski, G.D. Pollock, J.K. Swartzendruber, J. Hayes, Molecular structure of the dihydropyridazinone cardiotonic 1,3-dihydro-3,3-dimethyl-5-(1,4,5,6-tetrahydro-6-oxo-3-pyridazinyl)-2H-indol-2-one, a potent inhibitor of cyclic AMP phosphodiesterase, J. Med. Chem. 30 (1987) 623–627.
[21] S. Archan, W. Toller, Levosimendan: current status and future prospects, Curr. Opin. Anesthesiol. 21 (1) (2008) 78–84.
[22] Z. Lei, Introduction: ionic liquids, Chem. Rev. 117 (10) (2017) 6633–6635.
[23] K.S. Egorova, E.G. Gordeev, V.P. Ananikov, Biological activity of ionic liquids and their application in pharmaceutics and medicine, Chem. Rev. 117 (10) (2017) 7132–7189.
[24] (a) R.F.M. Elshaarawy, C. Janiak, Ionic liquid-supported chiral saldach with tunable hydrogen bonding: synthesis, metalation with Fe(III) and in vitro antimicrobial susceptibility, Tetrahedron 70 (43) (2014) 8023–8032;
(b) R.F.M. Elshaarawy, Z.H. Kheiralla, A.A. Rushdy, C. Janiak, New water soluble bis-imidazolium salts with a saldach scaffold: synthesis, characterization and in vitro cytotoxicity/ bactericidal studies, Inorg. Chim. Acta 421 (2014) 110–122;
(c) R.F.M. Elshaarawy, C. Janiak, Toward new classes of potent antibiotics: synthesis and antimicrobial activity of novel metallosaldach–imidazolium salts, Eur. J. Med. Chem. 75 (2014) 31–42.
[25] (a) . R.F.M. Elshaarawy, T.B. Mostafa, A.A. Refaee, E.A. El-Sawi, Ionic Sal-SG Schiff bases as new synergetic chemotherapeutic candidates: synthesis, metalation with Pd(II) and in vitro pharmacological evaluation, RSC Adv. 5 (2015) 68260–68269;
(b) R.F.M. Elshaarawy, C. Janiak, Antibacterial susceptibility of new copper(II)*N*-pyruvoyl anthranilate complexes against marine bacterial strains – in search of new antibiofouling candidate, Arab. J. Chem. 9 (2016) 825–834.
[26] (a) J.-Y. Lee, K.-W. Jeong, S. Shin, J.-U. Lee, Y. Kim, Antimicrobial natural products as β-ketoacyl-acyl carrier protein synthase III inhibitors, Bioorg. Med. Chem. 17 (2009) 5408–5413;
(b) H.J. Zhang, Z.L. Li, H.L. Zhu, Advances in the research of β-ketoacyl-ACP synthase III (FabH) inhibitors, Curr. Med. Chem. 19 (2012) 1225–1237.
[27] S.S. Khandekar, R.A. Daines, J.T. Lonsdale, Bacterial β-ketoacyl-acyl carrier protein synthases as targets for antibacterial agents, Curr. Protein Pept. Sci. 4 (2003) 21–29.
[28] (a) R.J. Heath, C.O. Rock, Regulation of fatty acid elongation and initiation by acyl-acyl carrier protein in *Escherichia coli*, J. Biol. Chem. 271 (1996) 1833–1836;
(b) J.-T. Tsay, W. Oh, T. Larson, S. Jackowski, C. Rock, Isolation and characterization of the beta-ketoacyl-acyl carrier protein synthase III gene (fabH) from *Escherichia coli* K-12, J. Biol. Chem. 267 (1992) 6807–6814.
[29] (a) C.E. Christensen, B.B. Kragelund, P. von Wettstein-Knowles, A. Henriksen, Structure of the human β-ketoacyl [ACP] synthase from the mitochondrial type II fatty acid synthase, Protein Sci. 16 (2007) 261–272;
(b) H.Q. Li, L. Shi, Q.S. Li, P.G. Liu, Y. Luo, J. Zhao, H.L. Zhu, Synthesis of C (7) modified chrysin derivatives designing to inhibit β-ketoacyl-acyl carrier protein synthase III (FabH) as antibiotics, Bioorg. Med. Chem. 17 (2009) 6264–6269.
[30] C.S. Ciobanu, S.L. Iconaru, P. Le Cousumer, L.V. Constantin, D. Predoi, Antibacterial activities of HAp-TiO_2 composites by Sol-Gel dip-coating technique, Nanoscale Res. Lett. 3 (2012) 27–35.
[31] (a) V. Pliska, B. Testa, H. Waterbeemd, Lipophilicity in Drug Action and Toxicology, VCH Publishers, New York, 1996;
(b) J. Sangster, Octanol-water Partition Coefficients: Fundamentals and Physical Chemistry, vol. 2, John Wiley & Sons, Chichester, 1997.
[32] A.J. Leo, CLOGP, Version 3.63, Daylight Chemical Information Systems, Irvine, CA, 1991.
[33] H.M. Berman, J. Westbrook, Z. Feng, G. Gilliland, T.N. Bhat, H. Weissig, I.N. Shindyalov, P.E. Bourne, The Protein Data Bank, Nucleic Acids Res. 28 (2000) 235–242.
[34] G.M. Morris, D.S. Goodsel, R.S. Halliday, R. Huey, W.E. Hart, R.K. Belew, A.J. Olson, Automated docking using a Lamarckian genetic algorithm and an empirical binding free energy function, J. Comput. Chem. 19 (1998) 1639–1662.
[35] Molecular Operating Environment (MOE). , Chemical Computing Group, Quebec, Canada, 2012http://www.chemcomp.com.
[36] (a) L.L. Dai, H.Z. Zhang, S. Nagarajan, S. Rasheed, C.H. Zhou, Synthesis of tetrazole compounds as a novel type of potential antimicrobial agents and their synergistic effects with clinical drugs and interactions with calf thymus DNA, Med. Chem. Commun. 6 (2015) 147–154;
(b) L. Huang, M. Terakawa, T. Zhiyentayev, Y.Y. Huang, Y. Sawayama, A. Jahnke, G.P. Tegos, T. Wharton, M.R. Hamblin, Innovative cationic fullerenes as broad-spectrum light-activated antimicrobials, Nanomedicine: NBM 6 (2010) 442–452.
[37] X. Qiu, C.A. Janson, W.W. Smith, M. Head, J. Lonsdale, A.K. Konstantinidis, Refined structures of beta-ketoacyl-acyl carrier protein synthase III, J. Mol. Biol. 307 (2001) 341–356.